Mesoporous Materials

Highly Ordered Mesoporous Bioactive Glasses with Superior In Vitro Bone-Forming Bioactivities**

Xiaoxia Yan, Chengzhong Yu, Xufeng Zhou, Jiawei Tang, and Dongyuan Zhao**

Bioactive glasses (BGs) have attracted much attention since the pioneering work by Hench et al. in 1971.[1] Glass ceramics with CaO-P_2O_5-SiO_2-MO (M = Na, Mg, etc) compositions have been widely studied and used in clinical applications because such materials can chemically bond with living bone.[2,3] The inorganic part of the human bone is hydroxycarbonate apatite (HCA), and when BGs are implanted in the human body an HCA layer with the ability to bond with living bone is formed on the surface of the bioactive material. For the sol–gel-derived BGs[4,5] to exhibit in vitro behaviour, it has been shown that both the composition and structure are important,[6–9] while melt-derived glasses show a direct dependence on composition. Increasing the specific surface area and pore volume of BGs may greatly accelerate the kinetic deposition process of HCA and therefore enhance the bone-forming bioactivity of BGs.[6] More importantly, precise control over porosity, pore size, and internal pore architecture of BGs on different length scales is essential for the understanding of the structure–bioactivity relationship and the rational design of better bone-forming biomaterials. However, a multicomponent glass system is quite complex and consists of mainly amorphous oxides, and thus the synthesis of ordered mesoporous BGs by using a well-studied surfactant-templating route[10] has not been reported. Herein we demonstrate that highly ordered mesoporous bioactive glasses (MBGs) have been successfully synthesized by templating with a block copolymer.[11] MBGs lead to superior bone-forming bioactivities in vitro compared to normal BGs derived from sol–gels. Moreover, the mesostructure of MBGs is also shown to be important with regard to their bioactivities. Such MBGs are important in both mesoporous material and biomaterial research and may open up new opportunities

[*] X. Yan, Prof. Dr. C. Yu, X. Zhou, J. Tang, Prof. Dr. D. Zhao
Department of Chemistry and
Shanghai Key Laboratory of Molecular Catalysis and
Innovative Materials
Fudan University
Shanghai 200433 (P. R. China)
Fax: (+86) 21-6564-1740
E-mail: czyu@fudan.edu.cn
dyzhao@fudan.edu.cn

[**] This work was financially supported by the National Science Foundations of China (20301004, 20233030, and 20173012), State Key Research Program (2002AA321010 and 001CB510202), and Shanghai Science Committee (0212 nm043, 0352 nm108, 03DJ14004, and 03QF14002).

Supporting information for this article is available on the WWW under http://www.angewandte.org or from the author.

  DOI: 10.1002/ange.200460598

in implanting, drug delivery, and as coating-materials in tissue engineering.[12–16]

Highly ordered MBGs were synthesized by using nonionic block copolymers as structure-directing agents[11] through an evaporation-induced self-assembly (EISA) process.[17] The powder X-ray diffraction (XRD) pattern of the calcined MBG 80S15C (80S and 15C represents the molar fraction of Si and Ca, respectively) shows three diffraction peaks in the small-angle regime ($2\theta = 1.19$, 2.11, 2.41°), which can be indexed to the (100), (110), and (200) diffractions of a two-dimensional hexagonal (*p6mm*) lattice with a cell parameter *a* of 8.50 nm (Figure 1a). Transmission electron microscope

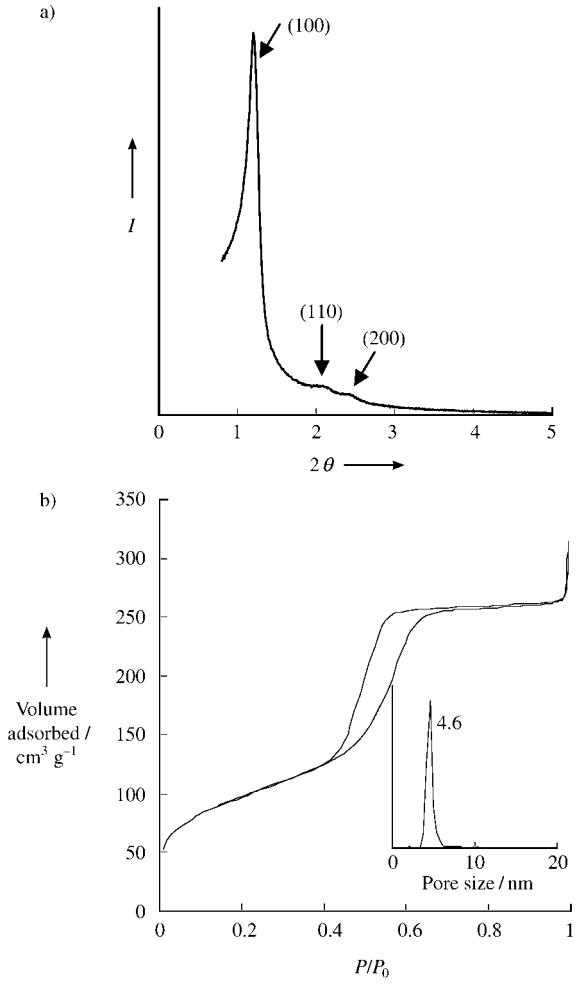

Figure 1. a) XRD pattern and b) N_2 sorption isotherm of calcined MBG 80S15C synthesized in the presence of P123 template. The inset shows a plot of the pore size distribution (calculated by BdB method).

(TEM) images along the [001] and [100] directions also reveal a highly ordered hexagonal arrangement of one-dimensional channels (Figure 2a and b, respectively). Nitrogen sorption isotherms further confirm the existence of uniform mesopores (Figure 1b). The BET surface area, pore volume, and pore size is calculated to be 351 $m^2 g^{-1}$, 0.49 $cm^3 g^{-1}$, and 4.60 nm, respectively. For comparison, calcined BG 80S15C synthesized without surfactants has a relatively lower pore volume of 0.067 $cm^3 g^{-1}$. MBGs synthesized in a range of compositions

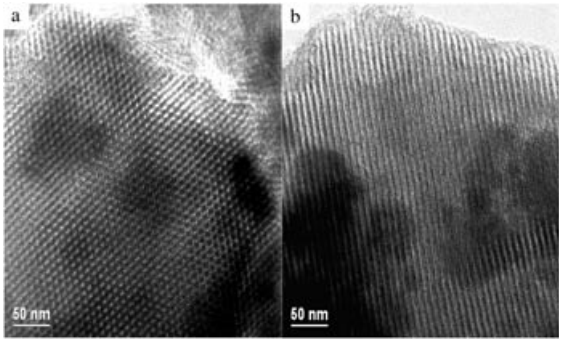

Figure 2. TEM images of calcined hexagonal MBG 80S15C recorded along the a) [001] and b) [100] directions.

by using P123 as the template in an EISA process possess ordered hexagonal structures. Furthermore, the pore sizes of MBGs can be tuned in the range of 4–7 nm by varying the structure-directing agent, for example, F127 or B50-6600. The physicochemical properties of the MBGs studied are summarized in Table 1.

Table 1: Physicochemical properties of MBGs and BGs.

	Structure	*d* (100) [nm]	BET surface area [$m^2 g^{-1}$]	Pore volume [$cm^3 g^{-1}$]	Pore size [nm]
100S-P123	*p6mm*	6.9	300	0.40	4.4
80S15C-P123	*p6mm*	7.4	351	0.49	4.6
70S25C-P123	*p6mm*	7.4	319	0.49	4.6
60S35C-P123	*p6mm*	6.9	310	0.43	4.3
70S25C-F127	wormlike	9.2	300	0.36	5.0
60S35C-B50-6600	wormlike	10.5	228	0.42	7.1
80S15C	–	–	9.8	0.07	–

Thermogravimetric analysis (TGA) and differential TGA (DTGA) curves for MBG 80S15C and BG 80S15C are shown in Figure 3. As the heating process proceeds, four clear mass losses are observed for BG samples between 18 and 150 °C, 150 and 300 °C, 300 and 430 °C, and 440 and 560 °C. For the MBG samples, two mass losses are observed between 25 and 125 °C as well as between 140 and 270 °C; a steep weight loss stage occurs between 300 and 325 °C. Larger mass losses (70 %, between 25 and 700 °C) are observed in the case of MBG compared to BG (55 %) as a result of the extra weight loss of the surfactants. A comparison of the TGA and DTGA profiles of two samples suggests that MBG samples are more homogenous in composition than BG samples.[18] The peak appearing around 300–325 °C most likely arises from the simultaneous decomposition of inorganic precursors and block copolymers.

Most of the previous syntheses of sol–gel-derived BGs were carried out under aqueous conditions, and a high-temperature (> 100 °C) drying process was required to remove the solvents; therefore, ordered MBGs were not

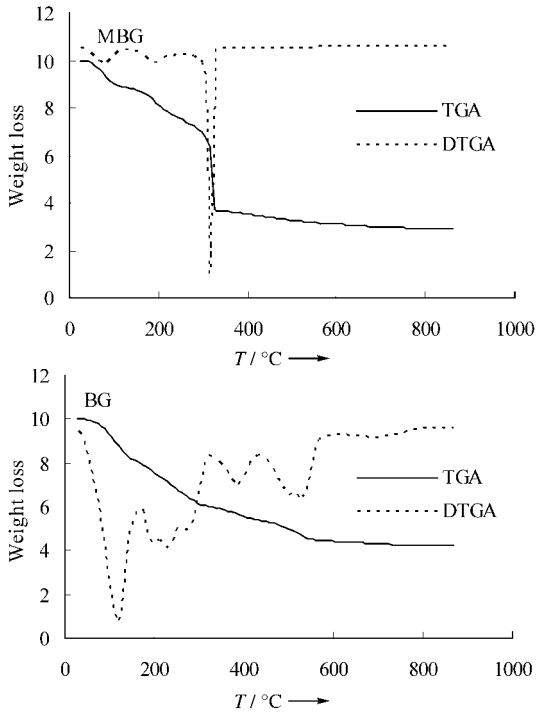

Figure 3. TGA and DTGA curves of MBG 80S15C obtained with a P123 template and BG 80S15C synthesized in the absence of surfactant.

obtained, even in the presence of surfactants. Performing the EISA process in near non-aqueous conditions in the current strategy is essential for the assembly of highly ordered MBGs. It is important to note that the MBGs fabricated in our study are unique compared to conventional BGs for the following two reasons. Firstly, the mechanism for the generation of the mesopore is different: Conventional BGs also possess mesopores which arise from the random distribution of CaO within the network of SiO_2.[6] The self-assembly of surfactants in MBGs gives rise to uniform mesopores as well as ordered mesostructures. To support this point, MBG 60S35C and 80S15C show similar N_2 adsorption isotherms and pore diameters (5.0 and 4.6 nm, respectively; see Table 1), while BG 60S35C and 80S15C synthesized by Vallet-Regi et al. have a mean pore size of 12 and 5 nm, respectively.[6] Accordingly, BG 80S15C shows H_2-type hysteresis loops associated with inkbottle-like pores[6] while MBG 80S15C shows H_1-type hysteresis loops typical of one-dimensional channels (Figure 1b). Secondly, the compositional homogeneity of the framework is different. The microphase separation and heterogeneity is common in normal sol–gel-derived BGs,[18] and is also observed in our BGs obtained by the EISA process. The TGA, energy dispersive spectroscopy (EDS), and scanning electron microscopy (SEM) results (see below) indicate that all the components are homogeneously distributed in the network in the case of MBGs. Since ordered mesostructured materials are formed by the regular packing of composite micelles on the nanometer scale, it is suggested that the homogeneous dispersion of inorganic species on this length scale may lead to a more homogeneous material (MBG) than conventional BGs. Inorganic salts have also been employed in the EISA process to produce macro- and mesoporous materials[19] as well as metal oxide nanowire arrays within mesostructured frameworks[20] where the crystallization of the salt/metal oxide and phase separation of a crystalline phase from amorphous sol–gel materials is unavoidable. In our case, the utilization of calcium nitrate in the synthesis gives rise to transparent monoliths and films before calcination (see Supporting Information), and a homogeneous glassy state is obtained after thermal treatment at 700 °C, as evidenced by wide-angle XRD measurements. It is important to note that the use of a nitrate salt and its subsequent decomposition during calcination is another essential factor in the fabrication of homogeneous MBGs.[21]

MBGs with high specific surface area and pore volume should have a greatly enhanced bone-forming bioactivity than conventional BGs.[6] It is believed that the prerequisite for glasses and glass ceramics to bond to living bone is the formation of a biologically active HCA layer on the surface of the BGs in the body. Therefore, the bone-forming activity of MBGs (and BG for comparison) in vitro was tested in simulated body fluid (SBF)[22] to monitor the formation of HCA on the surface of MBGs over time. SEM images of MBG 80S15C before soaking shows a smooth and homogenous surface (Figure 4a), which is in accordance with the results suggested by EDS and TGA analysis. The growth of nanoparticles (<100 nm in diameter) is observed after soaking the sample for 4 h (Figure 4b). It is surprising to note that a rodlike morphology (ca. 100 nm in length) which is similar to the morphology of HCA in human bones is exclusively observed after 8 h (Figure 4c). TEM examination reveals that such rods consist of even smaller nanorods about 5 nm in diameter (Figure 4g). EDS analysis shows that the molar ratio of Ca/P is 1.53:1 within such rods (Figure 4g, inset). Fourier transform infrared spectroscopy (FTIR) analysis of MBG 80S15C after immersing in SBF for 8 h shows the absorption bands of the phosphate group at 1040, 962, 603, and 562 cm^{-1}, together with the absorption bands of the carbonate group at 1488, 1432, and 870 cm^{-1}, which is in accordance with the IR spectra of HCA (see Supporting Information).[6] High-resolution TEM studies further confirms the existence of crystalline HCA nanorods (Figure 4h); however, some amorphous rodlike morphology is still observed, which is in agreement with the diffraction rings in the electron diffraction (ED) pattern (Figure 4h, inset). The rodlike morphology is maintained with increasing immersion time and the crystallinity of HCA increases as reflected by FTIR results (data not shown). EDS analysis shows a molar ratio of Ca/P = 1.66:1 in the rodlike HCA materials after seven days, a ratio almost equal to that of perfect HCA materials. The surface of BG 80S15C synthesized in the absence of surfactant and before soaking is heterogeneous (Figure 4d), which is very different from the MBG samples. The induction time for the formation of amorphous HCA and the subsequent deposition rate of HCA on the surface of BG is much slower than for MBG (Figure 4e, f), a result which is in accordance with the inductively coupled plasma (ICP) atomic emission spectroscopy results (see Supporting Information).[6,23] The rodlike HCA materials cannot be observed even after three days in the case of BG samples. It is

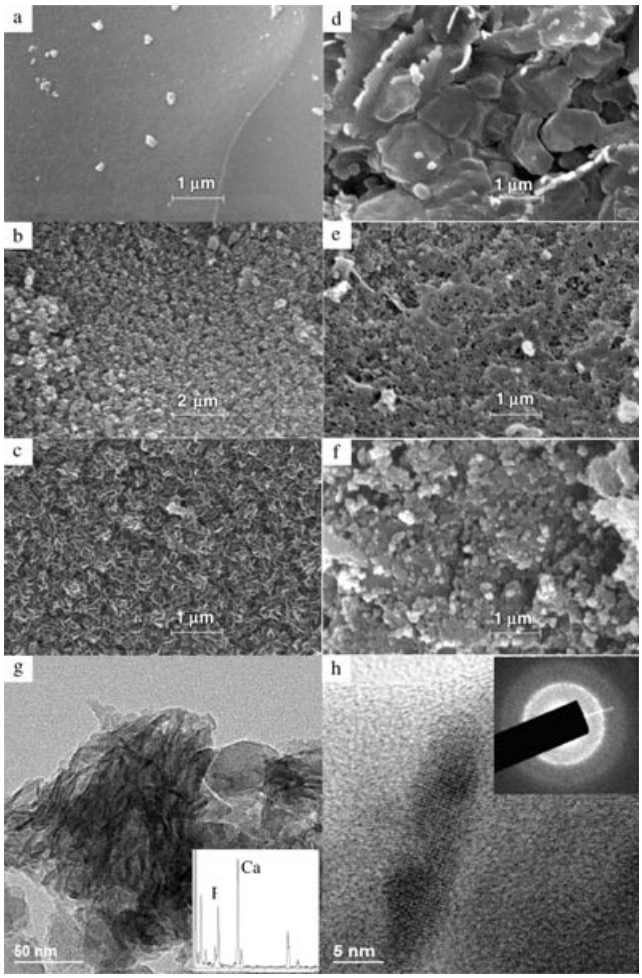

Figure 4. SEM images of MBG 80S15C (P123 template) after immersing in SBF for 0, 4, and 8 h (a)–(c). SEM images of BG 80S15C after soaking in SBF for 0, 8 and 48 h (d)–(f). TEM images of MBG 80S15C after soaking in SBF for 8 h at different magnifications (g) and (h). The EDS result (inset of g) and ED pattern (inset of h) of HCA deposited on MBG samples are also shown.

concluded that MBG with its larger pore volume and more accessible mesopore surface area has a much better bone-forming bioactivity in vitro than BG materials. The fast (ca. 8 h) and biomimetic HCA formation behavior (morphology of HCA similar to that in human body formed in simulated biological conditions) of MBGs means that the MBGs synthesized by the current strategy possess an outstanding bone-forming activity in vitro compared to other reported BGs.

The composition of MBGs is another important factor for their bioactivity. SEM results (see the Supporting Information) reveal that the bioactivity of MBGs in vitro follows the following sequence: 80S15C > 70S25C > 60S35C > 100S. The type of mesostructure in MBGs of the same composition is also important to the in vitro bioactivity. MBGs with the same composition (70S25C) have been synthesized in the presence of F127 and P123 (denoted MBG-F127 and MBG-P123, respectively) and their in vitro bioactivity compared. The dominant morphology of HCA deposited on MBG-P123 after immersing the MBG in SBF for 4 h is nanoparticles (see the Supporting Information), but a rodlike morphology is already observed in the case of MBG-F127 (see the Supporting Information). Since the composition, the pore volume, and pore size of both MBG materials are similar, the observed difference in bioactivity is most likely attributed to their pore structures (Table 1): MBG-F127 with 3-dimensional pore structures may facilitate the transportation of dissolved Ca^{2+} and O-Si-O species as well as the subsequent deposition of HCA materials. More importantly, since the pore size and pore structure is important in the protein-adsorption behavior for mesoporous materials,[24] it is believed that MBGs with a tunable pore size and pore structure may greatly influence the protein adsorption and nutrient delivery behavior for better in vivo bioactivity.

In conclusion, highly ordered mesoporous bioactive glasses have been synthesized with superior bone-forming bioactivity in vitro. Successful control of the mesostructure of MBGs adds a new dimension to the art of designed synthesis of bioactive glass materials. By carefully tuning the pore size, pore structure, and composition of MBGs, it is anticipated that MBGs with better in vivo bioactivity may be synthesized. MBGs with controllable morphologies may also be used for drug delivery, implant coating materials, and tissue engineering.

Experimental Section

MBGs were synthesized by using nonionic block copolymers such as $EO_{20}PO_{70}EO_{20}$ (P123), $EO_{106}PO_{70}EO_{106}$ (F127), and $EO_{39}BO_{47}EO_{39}$ (B50–6600) as structure-directing agents (EO is poly(ethylene oxide), PO is poly(propylene oxide), and BO is poly(butylene oxide)). In a typical synthesis of MBG, P123 (4.0 g), tetraethyl orthosilicate (TEOS, 6.7 g), $Ca(NO_3)_2{\cdot}4H_2O$ (1.4 g), triethyl phosphate (TEP, 0.73 g; Si/Ca/P = 80:15:5, molar ratio), and 0.5 M HCl (1.0 g) were dissolved in ethanol (60 g) and stirred at room temperature for 1 day. The resulting sol was introduced into a Petri dish to undergo an evaporation-induced self-assembly (EISA) process.[17] The dried gel was calcined at 700 °C for 5 h to obtain the final MBG products (denoted 80S15C according to the molar fraction of Si and Ca). For comparison, BG 80S15C was synthesized by an identical process but without surfactants.

MBG and BG materials were ground and sieved. Granules with sizes in 76–38 μm fractions were selected. The bone-forming activity of MBGs (and BGs) in vitro was tested by immersing selected granules (100 mg) in simulated body fluid (SBF, 100 mL)[22] to monitor the formation of HCA on the surface of MBGs over time. The solids were separated by filtration, washed three times with acetone, and dried in air.

Received: May 8, 2004

Keywords: bioinorganic chemistry · block copolymers · glasses · mesoporous materials · template synthesis

[1] L. L. Hench, R. J. Splinter, W. C. Allen, T. K. Greenlee, *J. Biomed. Mater. Res.* **1971**, *2*, 117.
[2] L. L. Hench, *J. Am. Ceram. Soc.* **1998**, *81*, 1705.
[3] L. L. Hench, J. M. Polak, *Science* **2002**, *295*, 1014.
[4] R. Li, A. E. Clark, L. L. Hench, *J. Appl. Biomater.* **1991**, *2*, 231.
[5] T. Peltola, M. Jokinen, H. Rahiala, E. Levanen, J. B. Rosenholm, I. Kangasniemi, A. Yli-Urpo, *J. Biomed. Mater. Res.* **1999**, *44*, 12.
[6] M. Vallet-Regi, C. V. Ragel, A. J. Salinas, *Eur. J. Inorg. Chem.* **2003**, 1029.

[7] M. M. Pereira, A. E. Clark, L. L. Hench, *J. Am. Ceram. Soc.* **1995**, *78*, 2463.
[8] M. Vallet-Regi, A. Ramila, *Chem. Mater.* **2000**, *12*, 961.
[9] M. Vallet-Regi, D. Arcos, J. Perez-Pariente, *J. Biomed. Mater. Res.* **2000**, *51*, 23.
[10] C. T. Kresge, M. E. Leonowicz, W. J. Roth, J. C. Vartuli, J. S. Beck, *Nature* **1992**, *359*, 710.
[11] D. Y. Zhao, J. L. Feng, Q. S. Huo, N. Melosh, G. H. Fredrickson, B. F. Chmelka, G. D. Stucky, *Science* **1998**, *279*, 548.
[12] L. L. Hench, *J. Biomed. Mater. Res.* **1998**, *41*, 511.
[13] P. Sepulveda, J. R. Jones, L. L. Hench, *J. Biomed. Mater. Res.* **2002**, *59*, 340.
[14] E. M. Santos, S. Radin, P. Ducheyne, *Biomaterials* **1999**, *20*, 1695.
[15] T. Kokubo, *Biomaterials* **1991**, *12*, 155.
[16] J. M. Gomez-Vega, A. Hozumi, H. Sugimura, O. Takai, *Adv. Mater.* **2001**, *13*, 822.
[17] C. J. Brinker, Y. F. Lu, A. Sellinger, H. Y. Fan, *Adv. Mater.* **1999**, *11*, 579.
[18] M. Jokinen, H. Rahiala, J. B. Rosenholm, T. Peltola, I. Kangasniemi, *J. Sol-Gel Sci. Technol.* **1998**, *12*, 159.
[19] D. Y. Zhao, P. D. Yang, B. F. Chmelka, G. D. Stucky, *Chem. Mater.* **1999**, *11*, 1174.
[20] H. F. Yang, Q. H. Shi, B. Z. Tian, Q. Y. Lu, F. Gao, S. H. Xie, J. Fan, C. Z. Yu, B. Tu, D. Y. Zhao, *J. Am. Chem. Soc.* **2003**, *125*, 4724.
[21] C. J. Brinker, G. W. Scherer, *Sol-gel science: the physics and chemistry of sol-gel processing*, Academic Press, New York, **1990**.
[22] T. Kokubo, H. Kushitani, S. Sakka, T. Kitsugi, T. Yamamuro, *J. Biomed. Mater. Res.* **1990**, *24*, 721.
[23] M. M. Pereira, L. L. Hench, *J. Sol-Gel Sci. Technol.* **1996**, *7*, 59.
[24] J. Fan, C. Z. Yu, T. Gao, J. Lei, B. Z. Tian, L. M. Wang, Q. Luo, B. Tu, W. Z. Zhou, D. Y. Zhao, *Angew. Chem.* **2003**, *115*, 3254; *Angew. Chem. Int. Ed.* **2003**, *42*, 3146.

